Supplemental Material for
Tailoring multi-loop atom interferometers with adjustable momentum transfer

L. A. Sidorenkov, R. Gautier, M. Altorio, R. Geiger and A. Landragin

LNE-SYRTE, Observatoire de Paris-Université PSL, CNRS,
Sorbonne Université, 61 avenue de l'Observatoire, 75014 Paris, France.

(Dated: September 22, 2020)

S1. PHASE SHIFTS OF THE SPURIOUS LOOPS

Given a macroscopic separation of the two spurious interferometers of about 2.5 mm at the detection moment, they do not interfere between each other and may be considered separately. Below we derive the phase shift of the bottom spurious interferometer (Fig. S1) at the moment of detection. As the calculation for the top spurious loop is conceptually similar, we only provide the final result. In the following, we neglect the finite time length of the laser

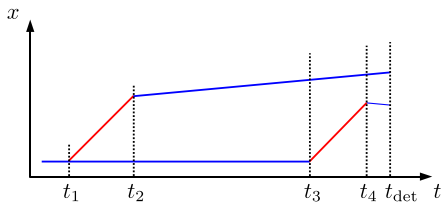

Figure S1. Sketch of the bottom spurious interferometer sequence until the detection moment. Vertical dashed lines indicate the four timings of the applied light pulses $\{t_i\}$ and of the detection pulse. Red (blue) color labels $F = 3$ ($F = 4$) internal state of the atoms. For clarity, we show only the output port corresponding to the $F = 4$ state.

pulses (all pulses have an area of $\pi/2$ and time length of 10 μs << 400 ms = T) and consider them applied at the time moments $t_1..t_4$ (see Fig. A1), while $t = 0$ moment corresponds to the launch of the atomic cloud:

$$\begin{aligned} t_1 &= 114 \text{ ms} \\ t_2 &= t_1 + T/2 - \Delta T \\ t_3 &= t_1 + 3T/2 + \Delta T + \Delta T_3 \\ t_4 &= t_1 + 2T \\ t_{\rm det} &= t_1 + 2T + \Delta t_{\rm det}, \end{aligned} \tag{S1}$$

where $\Delta T = 40$ μs is the initial time shift that separates in time the recombination moments of the main and spurious inerferometers (see main text and additional data section below), ΔT_3 is the delay of the third pulse and $\Delta t_{\rm det} = 70$ ms is the time interval past the last laser pulse until the detection moment ($t_{\rm det}$).

The total interferometric phase shift may be represented as a sum of three parts [1]:

$$\Delta\Phi = \Delta\Phi_{\rm las} + \Delta\Phi_{\rm prop} + \Delta\Phi_{\rm sep} \tag{S2}$$

Here $\Delta\Phi_{\rm las}$ is the laser phase which is imprinted onto the atomic wave-packet via interaction with Raman laser pulses; $\Delta\Phi_{\rm prop}$ is the free propagation phase difference accumulated along the paths; $\Delta\Phi_{\rm sep}$ is the phase shift arising from spatial separation of the two wave-packets at the moment of detection (interference), so-called separation phase. We take the convention for $\Delta\Phi$ being the phase shift of the upper branch minus the phase shift of the lower branch, and mark the related variables with u(l) subscripts.

Laser phase The laser phase reads as:

$$\begin{aligned}
\Delta\Phi_{\text{las}} &= (\varphi_1-\varphi_2)_{\text{u}} - (\varphi_3-\varphi_4)_{\text{l}} \\
\varphi_1 &= \vec{k}_{\text{eff}}\vec{r}_{\text{u}}(t_1) - \int_0^{t_1}\omega_{\text{eff}}(t)dt \\
\varphi_2 &= (1-\epsilon)\vec{k}_{\text{eff}}\vec{r}_{\text{u}}(t_2) - \int_0^{t_2}\omega_{\text{eff}}(t)dt \\
\varphi_3 &= (1-\epsilon)\vec{k}_{\text{eff}}\vec{r}_{\text{l}}(t_3) - \int_0^{t_3}\omega_{\text{eff}}(t)dt \\
\varphi_4 &= \vec{k}_{\text{eff}}\vec{r}_{\text{l}}(t_4) - \int_0^{t_4}\omega_{\text{eff}}(t)dt
\end{aligned} \tag{S3}$$

For completeness, we account here for the phase change due to the ramp of two-photon laser frequency to fulfill the resonance condition due to the Doppler shift: $\omega_{\text{eff}}(t) = \omega_0 - \alpha(t - T - t_1)$, where $\omega_0 = \omega_{hf} + \hbar k_{\text{eff}}^2/2m$ expresses the resonance condition for the atom at rest, namely at the apogee point of trajectory at $t = t_1 + T$. The ramp rate α is given by the projection of the gravity acceleration on the Raman beams in $\Delta\theta = 0$ configuration: $\alpha = k_{\text{eff}}\, g \sin(\theta_0)$. We also note that we orient the X-Z plane of our sensor (plane in which the area of the loops opens) towards the geographic West thus zeroing any possible contribution from the Earth rotation rate $\vec{\Omega}$.

We now consider an atom (wave-packet) with initial ($t = 0$) classical velocity $\vec{v}_0$ and position $\vec{r}_0$ and express the position of the wave-packet at the relevant time moments, along the upper and lower branch:

$$\begin{aligned}
\vec{r}_{\text{u}}(t_1) &= \vec{r}_0 + \vec{v}_0 t_1 + \frac{1}{2}\vec{g}t_1^2 \\
\vec{r}_{\text{u}}(t_2) &= \vec{r}_0 + \vec{v}_0 t_2 + \frac{1}{2}\vec{g}t_2^2 + \frac{\hbar\vec{k}_{\text{eff}}}{m}(t_2 - t_1) \\
\vec{r}_{\text{l}}(t_3) &= \vec{r}_0 + \vec{v}_0 t_3 + \frac{1}{2}\vec{g}t_3^2 \\
\vec{r}_{\text{l}}(t_4) &= \vec{r}_0 + \vec{v}_0 t_4 + \frac{1}{2}\vec{g}t_4^2 + \frac{\hbar\vec{k}_{\text{eff}}}{m}(1-\epsilon)(t_4 - t_3)
\end{aligned} \tag{S4}$$

We plug these formulae into the equations S3 and, with the use of explicit timings (Eqs. S1) and obtain the final result for the laser phase shift, where we neglect the terms of the orders of $O(\epsilon^2, \epsilon\Delta T/T, \epsilon\Delta T_3/T)$:

$$\begin{aligned}
&\Delta\Phi_{\text{las}} = \Delta\Phi_{\text{r}_0} + \Delta\Phi_{\text{v}_0} + \Delta\Phi_{\text{g}+\alpha} + \Delta\Phi_{\text{rec}} \\
&\Delta\Phi_{\text{r}}(r_0) = 2\vec{k}_{\text{eff}}\vec{r}_0\epsilon \\
&\Delta\Phi_{\text{v}}(v_0) = \vec{k}_{\text{eff}}\vec{v}_0(2\epsilon(T + t_1) - \Delta T_3) \\
&\Delta\Phi_{\text{g}+\alpha} = (\vec{k}_{\text{eff}}\vec{g} - \alpha)\Big(\frac{3}{4}T^2 - T\Delta T - \frac{3}{2}T\Delta T_3\Big) + \vec{k}_{\text{eff}}\vec{g}\Big(\epsilon\big(\frac{5}{4}T^2 + 2Tt_1 + t_1^2\big) - t_1\Delta T_3\Big) \\
&\Delta\Phi_{\text{rec}} = -\frac{\hbar k_{\text{eff}}^2}{m}\Delta T_3
\end{aligned} \tag{S5}$$

The terms $\Delta\Phi_{\text{r}}(r_0)$ and $\Delta\Phi_{\text{v}}(v_0)$ depend on the initial position and velocity of the wave-packet. The last term $\Delta\Phi_{\text{g}+\alpha}$ contains the dc-acceleration shift which is in the leading order compensated by the frequency ramp α.

Free propagation phase The free propagation phase is given by the integrals of the Lagrangian along the two corresponding classical paths [2]:

$$\begin{aligned}
\Delta\Phi_{\text{prop}} &= \int_u L(t)dt - \int_{\text{l}} L(t)dt \\
L(t) &= \frac{1}{2}mv(t)^2 - m\vec{g}\vec{r}(t)
\end{aligned} \tag{S6}$$

Considering as before an atom (wave-packet) with initial classical velocity $\vec{v}_0$ and position $\vec{r}_0$, we perform straightforward integration until the moment of detection and obtain (neglecting same higher-order terms as in the calculation for the laser phase):

$$\Delta\Phi_{\text{prop}} = \vec{k}_{\text{eff}}\vec{v}_0(\Delta T_3 + 2\epsilon(T + \Delta t_{\text{det}})) + \frac{\hbar k_{\text{eff}}^2}{2m}(\Delta T_3 + \epsilon T) \tag{S7}$$

Separation phase This contribution arises from the fact that one detects the interference between two wave-packets at a given location $\vec{r}$ in the detection region which has certain distances from the positions of the two classical trajectory points $\vec{r}_\mathrm{u}(t_\mathrm{det})$ and $\vec{r}_\mathrm{l}(t_\mathrm{det})$. The general expression for this phase shift reads [3]:

$$\begin{aligned}\Delta\Phi_\mathrm{sep} &= \frac{1}{\hbar}(\vec{p}_\mathrm{u}(\vec{r}-\vec{r}_\mathrm{u}) - \vec{p}_\mathrm{l}(\vec{r}-\vec{r}_\mathrm{l})) = \frac{1}{\hbar}(-\vec{p}_c\vec{\Delta r} + \vec{\Delta p}(\vec{r}-\vec{r}_c)) \\ \vec{p}_c &= \frac{\vec{p}_\mathrm{u}+\vec{p}_\mathrm{l}}{2}, \vec{\Delta p} = \vec{p}_\mathrm{u} - \vec{p}_\mathrm{l} \\ \vec{r}_c &= \frac{\vec{r}_\mathrm{u}+\vec{r}_\mathrm{l}}{2}, \vec{\Delta r} = \vec{r}_\mathrm{u} - \vec{r}_\mathrm{l}\end{aligned} \tag{S8}$$

The phase shift expression should be then integrated over the detection plane to obtain the full signal. The integration leaves unaffected the term proportional to the wave-packet separation $\vec{\Delta r}$, while the contribution of the second term depends on the difference of momenta $|\vec{\Delta p}|$ and the dimension of the detection region d. Assuming the mean position $\vec{r}_c$ at the center of detection region, we can define the critical condition when this phase contribution changes the sign and thus start to rapidly vanish due to the averaging: $(|\vec{\Delta p}|/\hbar)\cdot(d/2) = \pi/2$. In our case, $|\vec{\Delta p}|/\hbar = 2\epsilon k_\mathrm{eff}$ and $d = 30$ mm, which gives a critical value of $\epsilon_\mathrm{crit} = 3.8\cdot 10^{-6}$. In the region of $\epsilon \sim \epsilon_\mathrm{crit}$ this contribution might cause some varying phase shift bias. Understanding these variations requires further modeling that is outside the scope of the present work. This bias is, however, suppressed by at least an order of magnitude for the region $\epsilon \simeq 10\ \epsilon_\mathrm{crit} = 0.4\cdot 10^{-4}$ that covers about 80% of the probed ϵ-span. We therefore neglect this contribution and obtain:

$$\Delta\Phi_\mathrm{sep} = -\frac{m\vec{v}_0}{\hbar}(\vec{r}_\mathrm{u}(t_4) - \vec{r}_\mathrm{l}(t_4) + 2\epsilon\frac{\hbar\vec{k}_\mathrm{eff}}{m}\Delta t_\mathrm{det}) = -\vec{k}_\mathrm{eff}\vec{v}_0(\Delta T_3 + 2\epsilon(T+\Delta t_\mathrm{det})) \tag{S9}$$

Note, that this expression is identical to the first term of $\Delta\Phi_\mathrm{prop}$ (Eq. (S7)) but with an opposite sign, as one may expect for a case of Lagrangian being quadratic in position and momentum [4]. In particular, the dependence in the timing between the final beam-splitter pulse and the detection, Δt_det, drops out when summing the two contributions.

We now combine all the results obtained above and express the full phase shift of the bottom spurious interferometer:

$$\Delta\Phi^{(\mathrm{B})} = \Delta\Phi_\mathrm{r}(r_0) + \Delta\Phi_\mathrm{v}(v_0) + \Delta\Phi_{\mathrm{g}+\alpha} + \frac{\hbar k_\mathrm{eff}^2}{2m}(T\epsilon - \Delta T_3) \equiv \Delta\Phi_{\mathrm{r}_0} + \Delta\Phi_{\mathrm{v}_0} + \Delta\Phi' - \frac{\hbar k_\mathrm{eff}^2}{2m}T\epsilon \tag{S10}$$

with $\Delta\Phi' = \Delta\Phi_{\mathrm{g}+\alpha} + \frac{\hbar k_\mathrm{eff}^2}{2m}(2T\epsilon - \Delta T_3)$ being the mean phase shift independent of the initial atomic position and velocity. A fully identical calculation for the top spurious loop retrieves the same dephasing in all but recoil parts:

$$\Delta\Phi^{(\mathrm{T})} = \Delta\Phi_\mathrm{r}(r_0) + \Delta\Phi_\mathrm{v}(v_0) + \Delta\Phi_{\mathrm{g}+\alpha} + \frac{\hbar k_\mathrm{eff}^2}{2m}(3T\epsilon - \Delta T_3) \equiv \Delta\Phi_{\mathrm{r}_0} + \Delta\Phi_{\mathrm{v}_0} + \Delta\Phi' + \frac{\hbar k_\mathrm{eff}^2}{2m}T\epsilon \tag{S11}$$

The total phase shifts of the two spurious loops are thus slightly different, such that $\Delta\Phi^{(\mathrm{T})} - \Delta\Phi^{(\mathrm{B})} = \frac{\hbar k_\mathrm{eff}^2}{m}T\epsilon$. This difference arises from the recoil terms in the free propagation contribution and vanishes for $\epsilon \to 0$.

S2. CONTRAST OF THE SPURIOUS LOOPS

The employed fluorescence detection in our apparatus does not discriminate the signals coming from two spurious loops. The total peak-peak contrast is therefore given by an incoherent sum of the two spurious signals. Considering the wave-packet with initial classical velocity $\vec{v}_0$ and position $\vec{r}_0$ we write:

$$C = \left[\frac{C^{(\mathrm{B})}}{2}\cos\Delta\Phi^{(\mathrm{B})} + \frac{C^{(\mathrm{T})}}{2}\cos\Delta\Phi^{(\mathrm{T})}\right]_\mathrm{pp}, \tag{S12}$$

with phase shifts $\Delta\Phi^{(\mathrm{B})}$ and $\Delta\Phi^{(\mathrm{T})}$ defined in Equations S10, S11 and $[...]_\mathrm{pp}$ denoting the peak-peak variation, and $C^{(\mathrm{B})}$ ($C^{(\mathrm{T})}$) being the contrasts of the bottom (top) spurious interferometer. We introduce the mean contrast $C_0 = \frac{(C^{(\mathrm{B})}+C^{(\mathrm{T})})}{2}$, the contrasts imbalance $\Delta C_0 = C^{(\mathrm{T})} - C^{(\mathrm{B})}$, the mean dephasing $\overline{\Delta\Phi} = \frac{\Delta\Phi^{(\mathrm{T})}+\Delta\Phi^{(\mathrm{B})}}{2}$, and recall that $\Delta\Phi^{(\mathrm{T})} - \Delta\Phi^{(\mathrm{B})} = \frac{\hbar k_\mathrm{eff}^2}{m}T\epsilon$. The Equation S12 becomes:

$$C = C_0 \left[\cos \overline{\Delta\Phi} \cos\left(\frac{\hbar k_{\text{eff}}^2}{2m} T\epsilon \right) - \frac{\Delta C_0}{C_0} \sin \overline{\Delta\Phi} \sin\left(\frac{\hbar k_{\text{eff}}^2}{2m} T\epsilon \right) \right]_{\text{pp}} \tag{S13}$$

The observed contrasts of both spurious loops results from the averaging over the same initial velocity and position distributions in the atomic cloud. Assuming fully uncorrelated normal velocity ($\propto e^{-v_0^2/2\sigma_v^2}$) and position ($\propto e^{-r_0^2/2\sigma_r^2}$) distributions, we average the velocity- and position-dependent parts of the mean phase $\overline{\Delta\Phi}$ in Eq. S13 and obtain normalized full peak-peak contrast as:

$$\begin{aligned} \frac{C(\epsilon, \Delta T_3)}{2C_0} &= \exp\left(-\frac{(2k_{\text{eff}}\sigma_r\epsilon)^2}{2} \right) \times \exp\left(-\frac{(k_{\text{eff}}\sigma_v(2\epsilon(T+t_1) - \Delta T_3))^2}{2} \right) \times \\ &\times \frac{1}{2} \left[\cos \Delta\Phi' \cos\left(\frac{\hbar k_{\text{eff}}^2}{2m} T\epsilon \right) - \frac{\Delta C_0}{C_0} \sin \Delta\Phi' \sin\left(\frac{\hbar k_{\text{eff}}^2}{2m} T\epsilon \right) \right]_{\text{pp}} \end{aligned} \tag{S14}$$

In Figure S2 we show the fit of the data with the general-case model of Eqn. S14, where mean peak contrast C_0, contrast imbalance ΔC_0 and standard deviation σ_r are free parameters (solid red line). We extract the values of $\sigma_r = 0.51(2)$ mm, $2C_0 = 0.934(18)$ and $\Delta C_0 = 0.03(3)\%$. The value of $2C_0 < 1$ simply accounts for the actual over-estimation of the maximum contrast resulting from data normalization to the maximum of the recorded contrasts. The fitted contrast imbalance $\Delta C_0 = 0.03(3)\%$ is well compatible with zero. Comparing this fit with the fit by simplified model used in the main text (dashed black line, for $\Delta C_0 = 0$) shows a small difference around the contrast local minimum at $\epsilon = 0.76 \cdot 10^{-4}$, without any change for the rest of the probed ϵ-values. Thus, all the arguments presented in the main text remain true for the case of the fit with exact function accounting for small contrast imbalance of the two spurious interferometers.

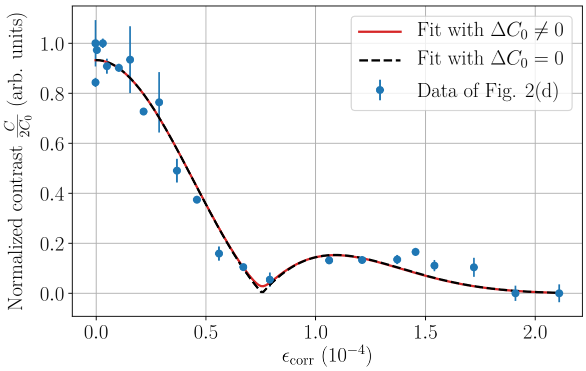

Figure S2. Normalized contrast of the spurious interferometers (data of Fig. 2(d), blue dots), fitted with exact model of Eqn. S14 (solid red line) and simplified model (Eqn. S14 with $\Delta C_0 = 0$, dashed black line), for comparison.

S3. ADDITIONAL DATA ON SPURIOUS INTERFEROMETERS

Time-domain width In Figure S3 we show the extracted the time-domain widths of the spurious interferometric peaks σ_t for all data sets similar to those of the Figure 2(b). The data shows a rather large scatter for the probed range of $\Delta\theta$ which is likely to come from an hour-timescale experimental variations, and day-to-day drifts in case of different data sets. In overall, we cannot identify any clear systematic trend and the behavior seems consistent with the expected independence of $\Delta\theta$. We thus obtain a weighted mean value of $\bar{\sigma}_t = 10.6(1.3)$ μs (dashed black line in Fig. S3) that we use to empirically set the value of $\sigma_v = 1/k_{\text{eff}}\bar{\sigma}_t = 1.8(2)$ v_R, where v_R is the single-photon atom recoil velocity. This value differs from the initial thermal width of $3.0(2)$ v_R, underlining the impact of the velocity-selection during the interrogation pulses.

Time-separation of the spurious and main interferometers While studying controlled recombination of the spurious interferometers, it is important to verify that the main interferometer is sufficiently distant such that its

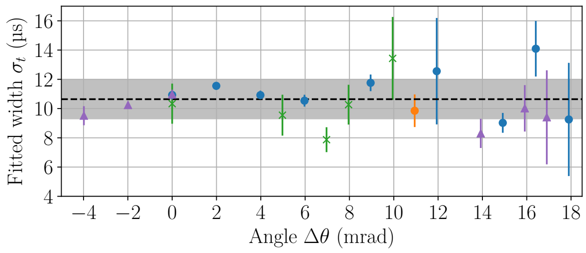

Figure S3. Fitted time-domain width of the spurious peaks for the probed values of $\Delta\theta$. Various symbols and accompanying colors indicate data sets taken on different days within two-week period. The dashed black line (gray-shaded area) are the weighted mean (standard deviation interval) of all shown data.

wings do not affect the spurious signal. In Figure S4(a) we plot the expected peak recombination time moment for spurious (same as solid black line in Fig. 2(c) of the main text) and main interferometers. These functions are given by: $\Delta T_3 = (T + t_1)\Delta\theta^2$ (spurious interferometer, solid blue line) and $\Delta T_3 = -2\Delta T + \frac{T}{2}\Delta\theta^2$ (main interferometer, dashed orange line), with $\Delta T = 40$ μs being an initial time shift of the second and third pulses as explained in the main paper. The timing separation between two peaks, therefore, is minimal and equals $2\Delta T$ for $\Delta\theta = 0$ and increases with increasing $|\Delta\theta|$. In Figure S4(b) we demonstrate that the choice of $\Delta T = 40$ μs excludes any overlap between the two peaks for $\Delta\theta = 0$.

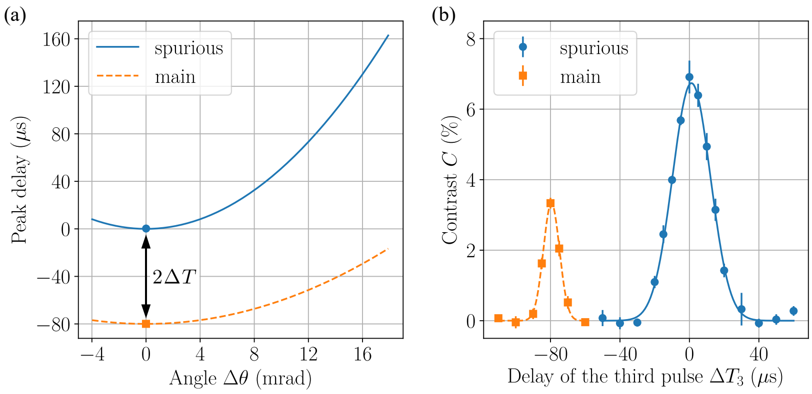

Figure S4. (a) Expected peak delay for spurious (solid blue line) and main (dashed orange line) interferometers as a function of $\Delta\theta$, for initial time separation $\Delta T = 40$ μs. The blue dot and orange square mark the expected peak positions for the data shown in the panel (b). (b) Peak-peak contrast of the spurious (blue dots) and main (orange squares) as a function of the third laser pulse delay ΔT_3, for $\Delta\theta = 0$, and Gaussian fits (solid blue and dashed orange lines) to the corresponding data.

S4. PHASE SHIFT OF THE MAIN LOOP

Sensitivity to rotation rate We derive the sensitivity to rotation rate of the main double-loop interferometer for the perfectly recombined symmetric configuration considered in the main paper using three different methods: the ABCD-matrix formalism [4], the full phase shift calculation approach (similar to the one of spurious intrferometers), and the geometric approach of Sagnac area calculation. All methods give the same result:

$$\Delta\Phi_\Omega = \frac{1}{2}\vec{k}_{\text{eff}}(\vec{g} \times \vec{\Omega})T^3 \left(1 - \frac{2\epsilon}{3}\right) \tag{S15}$$

Sensitivity to frequency An additional phase shift may arise in the AMT configuration if the effective laser frequency is detuned from the resonance condition at the apogee point of the fountain trajectory by a fixed amount $\Delta\omega_0$. This so-called clock shift can be estimated with by accounting for the frequency contribution to the imprinted laser phase (similarly to the above calculation for the spurious interferometers), or via sensitivity function [5] approach. In the limit of infinitely short laser pulses, we obtain:

$$\Delta\Phi_{\text{clock}} = 4\Delta\omega_0\Delta T_{\text{s}} = \Delta\omega_0\frac{2T\epsilon}{(1-\epsilon)} \approx \Delta\omega_0 T\Delta\theta^2 \tag{S16}$$

To quantify the clock sensitivity, we record the induced phase shift from the controlled change of the two-photon detuning for a set of different angles. The phase shift $\Delta\Phi_{\text{HS}}$ is evaluated as a half-sum (HS) of the measured values for alternating sign of $\vec{k}_{\text{eff}}$ and shows the expected linear dependence on frequency detuning $\Delta\omega_0$ (Fig. S5(a)). The fitted linear slopes $d\Delta\Phi_{\text{HS}}/d(\Delta\omega_0/2\pi)$ scale quadratically with $\Delta\theta$ (blue dots in Fig. S5(b)), well matched with the expectation from Eq. S16 (solid black line). As the clock shift is independent on $\vec{k}_{\text{eff}}$, it should vanish (or be significantly suppressed) in the half-difference (HD) signal of $\pm k_{\text{eff}}$ method that leaves unaffected the inertial shifts. The orange squares in Figure S5(b) show the corresponding clock sensitivity given by $d\Delta\Phi_{\text{HD}}/d(\Delta\omega_0/2\pi)$, boosted by a factor of 10 (including the error bars) for better visibility. We estimate a suppression factor ranging from about 10 (at 5 mrad) to better than 100 (at 20 mrad).

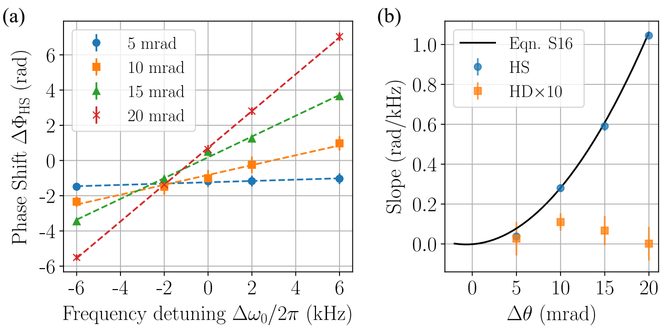

Figure S5. (a) Sensitivity of the main interferometer to the two-photon frequency in the AMT scheme, for different values of $\Delta\theta$, as extracted from the half-sum (HS) of the $\pm k_{\text{eff}}$ measurements. The solid blue, dashed orange, dash-dotted green and dotted red curves are linear fits to the corresponding data. (b) The fitted slopes $d\Delta\Phi/d(\Delta\omega_0/2\pi)$ of the half-sum signal of panel (a) and half-difference signal (HD), as a function of probed $\Delta\theta$. The solid black line indicates the expectation given by the Eqn. S16 for $\epsilon = \epsilon_{\text{calc}}$. The HD data and error bars are increased by a factor of 10 for visibility.

[1] Peter Wolf, Luc Blanchet, Christian J Bordé, Serge Reynaud, Christophe Salomon, and Claude Cohen-Tannoudji, "Does an atom interferometer test the gravitational redshift at the compton frequency?" Classical and Quantum Gravity **28**, 145017 (2011).

[2] Pippa Storey and Claude Cohen-Tannoudji, "The feynman path integral approach to atomic interferometry. a tutorial." J. Phys. II France **4**, 1999–2027 (1994).

[3] David Marvin Slaughter Johnson, Long baseline atom interferometry, Ph.D. thesis, Stanford University (2011).

[4] Ch. Antoine and Ch. J. Bordé, "Quantum theory of atomic clocks and gravito-inertial sensors: an update," Journal of Optics B: Quantum and Semiclassical Optics **5**, S199–S207 (2003).

[5] P. Cheinet, B. Canuel, F. Pereira Dos Santos, A. Gauguet, F. Yver-Leduc, and A. Landragin, "Measurement of the sensitivity function in a time-domain atomic interferometer," IEEE Transactions on Instrumentation and Measurement **57**, 1141–1148 (2008).